Performance of Synchronous Machine Models in a Series-Capacitor Compensated System

Shashidhara M. Kotian and K. N. Shubhanga

***Abstract*—This paper compares the IEEE-specified generator models such as the equivalent circuit (EC) models and the operational inductance (OI) models to understand their damping performances in the IEEE first-benchmark system for subsynchronous resonance study. These models are found to differ from one another only to an extent they accurately represent the standard transfer functions. By carrying out different case studies an effort is made to analyze the influence of these differences among the models on the damping performance of swing-mode and torsional modes. Through a detailed eigenvalue analysis and time-domain simulations, it is demonstrated that these models offer differing results with respect to swing-mode, thereby strongly influencing the power system stabilizer (PSS) performances, especially when the system is series compensated. Even the torsional mode interactions are found to exhibit dependency on the models employed for the generators. Such a study is expected to provide better insight into the behavior of generator models and controller design/tuning in system analysis.**

***Index Terms*—Eigenvalue analysis, modal speeds, subsynchronous resonance, synchronous machine models.**

I. Introduction

In a stability constrained power system, fixed series capacitor (FSC) compensation of transmission lines has been the natural choice for improving the power transfer capability [1]. However, such schemes are found to cause subsynchronous resonance (SSR) problems with turbogenerators involving torsional mode interactions depending on the compensation level [2]–[7]. To analyze SSR, eigenvalue-based approach is generally preferred [5], [6], as it gives better insight into the hidden modes associated with the system and complements the time-domain-based analysis. These studies provide information to design different countermeasures for mitigating the SSR [2]. However, carrying out such studies is not straightforward as it involves detailed modeling of power system components, more importantly the synchronous machines. In this regard, there has been a continued effort to suggest different models for synchronous machines for power system applications [8]–[21]. They are generally classified as phase-domain (PD), voltage-behind-reactance (VBR), and $dq0$-based models. The PD model [8]–[12] is expressed in terms of the machine's physical variables and phase coordinates. As in the PD model, in the VBR model [13]–[17], the stator circuit is represented in phase coordinates; but the rotor subsystem in dq rotor reference frame. These models are found to provide an accurate representation of internal machine phenomena, for example, stator inter-turn and/or inter-windings faults [8], [14]. The $dq0$ model [5]–[7], [22] which uses Park's transformation eliminates the problem of time-varying inductances that exist in the PD and VBR models, and therefore, has found wide applications in most of the nodal analysis-based EMTP-type of packages (such as ATP [23], MicroTran [24], PSCAD/EMTDC [25], EMTP-RV [26], etc.) and state-variable-based simulation packages (such as MATLAB/Simulink [27], Eurostag [28], Simpow, PSS/E [29], DIgSILENT PowerFactory [30], PowerWorld [31], etc.). Also, it is shown in [21] that the $dq0$ model performs identical to PD and VBR models for system-level transients analysis under unbalanced (as well as balanced) conditions.

The IEEE standard 1110-2002 [32] has suggested two major categories of $dq0$ models: equivalent circuit-based models (EC-model) and operational inductance-based models (OI-model). These model variations are suggested in an attempt to arrive at a state-model which truly represents the standard transfer functions $X_d(s)$ and $G(s)$ for d-axis and $X_q(s)$ for q-axis [32], and simultaneously map to the original state variables as far as possible. Such a transfer function-based (*lumped-parameter*) model is preferred for most of the *system-side* transient analysis [3], [21], [33], [34] as it captures the full details of the synchronous generator without requiring to use the basic coupled-circuit time-varying parameters. These transfer functions are obtained by conducting the IEEE standard-specified tests such as standstill frequency response (SSFR) tests in addition to many other open- and short-circuit tests [35]. In the EC-model [5], a circuit-model is derived to obtain a state-space model. Here, the circuit parameters are evaluated from the standard parameters (-transient and subtransient reactances and time constants) by employing a *classical data conversion* procedure [36], [37]. This leads to a synchronous machine model where neither of the transfer functions is accurately represented. This EC-model has been found to be used widely in most of the industry-grade software packages [27]–[31] since the procedure is straightforward to implement. It is also noted that in EMTP-kind of packages [23]–[26], an involved data conversion procedure, referred to as *Canay/Refined Canay data conversion*, is employed to arrive at a circuit-model which fits $X_d(s)$ accurately [38]–[40]. However, such a procedure is found to provide a close fit of the given $G(s)$ in most of the cases though not exact. In contrast

Manuscript received September 11, 2012; revised February 07, 2013, July 18, 2013, and October 23, 2013; accepted November 22, 2013. Date of publication December 17, 2013; date of current version April 16, 2014. Paper no. TPWRS-01039-2012.

The authors are with the Department of Electrical Engineering, National Institute of Technology Karnataka Surathkal, Mangalore, Karnataka 575025, India (e-mail: knsa1234@yahoo.com).

Digital Object Identifier 10.1109/TPWRS.2013.2292977

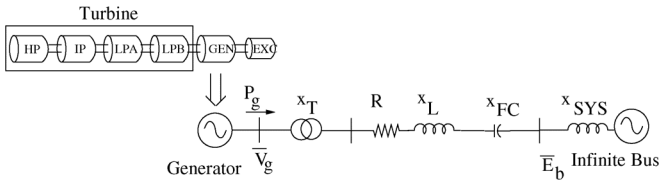

Fig. 1. IEEE first benchmark model.

to EC-model, in OI-model [6], a state-model is derived directly in terms of the standard parameters. In the basic OI-model, only $X_d(s)$ is accurately represented. However, in a refined OI-model [41] (referred to as OIR-model in this paper), both $X_d(s)$ and $G(s)$ are perfectly represented, giving an accurate model for the machine.

In this paper, a comparative study has been carried out to understand the small-signal performance of the EC-models and the OI-models with respect to the IEEE first-benchmark system (FBS) for SSR study [42], which is characterized by many torsional modes that are distributed in a relatively wide frequency range. Though parametric kind of analysis is well documented in the literature [43] related to the IEEE FBS, this paper highlights the influence of these synchronous machine models on the damping performance of both torsional and swing modes and in turn on the effectiveness of damping controllers, especially when the system is FSC compensated. The paper is structured as follows. Section II provides system details and introduces these synchronous generator models for ready reference. The results of the eigenvalue analysis along with time-domain simulations to validate the eigen-predictions for various cases are presented in Sections III–V.

II. System Details and Comparison of Synchronous Machine Models

Fig. 1 shows the IEEE first benchmark system used in the SSR analysis [42]. One damper, h, and field winding, f, on the d-axis, while on the q-axis two damper windings g and k are considered. System details such as generator standard parameters and the mechanical damping employed are provided in Appendix A for ready reference.

In the following lines, the EC-models and the OI-models are discussed briefly *only for d-axis*. The d-axis flux-linkage equation is given by

$$\psi_d(s) = X_d(s) i_d(s) + G(s) E_{fd}(s) \tag{1}$$

where the standard transfer functions are given by

$$X_d(s) = x_d \frac{(1+sT'_d)(1+sT''_d)}{(1+sT'_{do})(1+sT''_{do})} \tag{2}$$

$$G(s) = \frac{(1+sT_{kd})}{(1+sT'_{do})(1+sT''_{do})}. \tag{3}$$

A. EC-Model

In this case, the generator modeling involves the determination of the basic parameters such as the field/damper winding resistances and their respective leakage reactances from the standard parameters and the specified stator leakage reactance x_l using the classical data-conversion procedure indicated in Appendix B [5], [36]. In this procedure, it is assumed that the field resistance is zero while evaluating the damper winding resistance and when the field circuit resistance is determined the damper winding is assumed to be open-circuited. Thus, this approach provides a straightforward method to choose state variables which can be mapped directly to the actual machine variables, say, field current, h-damper winding current etc. However, this simplified process leads to an inaccurate representation of both the standard transfer functions $X_d(s)$ and $G(s)$.

B. OI-Model

In this case, to arrive at state-model, (1) is re-written as

$$i_d(s) = \frac{\psi_d(s)}{X_d(s)} - \frac{G(s)}{X_d(s)} E_{fd}(s) \tag{4}$$

where as per the IEEE standard [32], $1/X_d(s)$ is given by

$$\frac{1}{X_d(s)} = \frac{1}{x_d} + \left(\frac{1}{x'_d} - \frac{1}{x_d}\right)\frac{sT'_d}{1+sT'_d} + \left(\frac{1}{x''_d} - \frac{1}{x'_d}\right)\frac{sT''_d}{1+sT''_d}. \tag{5}$$

The short-circuit time-constants are derived by using (6) and (7)—see Appendix C. Further, to arrive at a state-model which maps truly to the original machine variable, it is assumed that $T_{kd} = T''_d$ in (3). This leads to a simplified OI-model where only $X_d(s)$ is exact. A partial set of state equations (only for d-axis) is listed below [6]:

$$\frac{d\psi_f}{dt} = \frac{1}{T'_d}\left[-\psi_f + \psi_d + \frac{x'_d}{x_d - x'_d} E_{fd}\right]$$
$$\frac{d\psi_h}{dt} = \frac{1}{T''_d}\left[-\psi_h + \psi_d\right].$$

C. OIR-Model

In this case, an attempt is made to derive a state-model representing accurately $X_d(s)$ as well as $G(s)$ unlike in the OI-model. It is to be noted that the realization of the OIR-model requires the value of T_{kd} which is not generally specified along with the set of the standard parameters. Therefore T_{kd} is approximately determined using the available standard parameters as per the IEEE-specified equation—see Appendix D. A partial set of state equations (only for d-axis) is listed below:

$$\frac{d\psi_F}{dt} = \frac{1}{T'_d}\left[-\psi_F + \psi_d + \frac{T'_d - T_{kd}}{T'_d - T''_d}\frac{x'_d}{x_d - x'_d} E_{fd}\right]$$
$$\frac{d\psi_H}{dt} = \frac{1}{T''_d}\left[-\psi_H + \psi_d + \frac{T''_d - T_{kd}}{T''_d - T'_d}\frac{x'_d x''_d}{x_d\,(x'_d - x''_d)} E_{fd}\right].$$

Note that though this approach provides an accurate state-space model of a synchronous generator, the state variable, say, ψ_H, does not map directly to the h-damper coil flux-linkage.

To enable comparison of the above said synchronous machine models, the standard transfer functions applicable to d-axis such as $X_d(s) = \psi_d(s)/i_d(s)$ and $G(s) = \psi_d(s)/E_{fd}(s)$ are derived for each model employing 2.2 model for the generator [5], [32]. These transfer functions are listed in Table I. From

TABLE I
GENERATOR-MODEL TRANSFER FUNCTIONS

Model	$X_d(s)$	$G(s)$
EC-model	$1.79\frac{(1+0.4744s)(1+0.0219s)}{(1+5.4662s)(1+0.0252s)}$	$\frac{(1+0.0041s)}{(1+5.4662s)(1+0.0252s)}$
OI-model	$1.79\frac{(1+0.4s)(1+0.0259s)}{(1+4.3s)(1+0.032s)}$	$\frac{(1+0.0259s)}{(1+4.3s)(1+0.032s)}$
OIR-model	$1.79\frac{(1+0.4s)(1+0.0259s)}{(1+4.3s)(1+0.032s)}$	$\frac{(1+0.00416s)}{(1+4.3s)(1+0.032s)}$
EC(Canay)	$1.79\frac{(1+0.4s)(1+0.0259s)}{(1+4.3s)(1+0.032s)}$	$\frac{(1+0.00356s)}{(1+4.3s)(1+0.032s)}$

the tabulated results, it can be seen that the EC-model leads us to open/short-circuit time-constants which differ significantly from the standard values. For example, T'_{do}/T''_{do} is obtained as 5.4662/0.0252 s, whereas the standard value is 4.3/0.032 s. However, in the OI-model, $X_d(s)$ is exact; whereas with OIR-model, both $X_d(s)$ and $G(s)$ are accurately represented.

D. EC(Canay)-Model

In this model, Canay data-conversion procedure [39] is employed to determine the circuit parameters—see Appendix E. The standard transfer functions for this EC-model are also shown in Table I. It is evident from the table that the EC(Canay) is almost identical to the OIR-model with an insignificant difference in T_{kd}.

Note:

1) The OIR-model turns out be *exactly identical* to the EC(Canay) if T_{kd} obtained in this EC-model is directly utilized in the OIR-model instead of that given by (8).
2) It should be noted that the synchronous machine models as shown above differ from one another (with respect to the standard transfer functions) only when the detailed models, i.e., 2.2. models are employed. When a reduced order model (with no rotor winding or at the most, one rotor winding on each of the d- and q-axes; e.g., 1.1, 1.0 or 0.0) is employed, all the four synchronous machine models become identical. In other words, the standard transfer functions turn out to be the same for all the four models and are given below:

$$X_d(s) = 1.79\frac{(1+0.4059\text{ s})}{(1+4.3\text{ s})} \text{ and } G(s) = \frac{1}{(1+4.3\text{ s})}.$$

Thus, it is clear that the differences between the models are only with respect to the standard transfer functions, $X_d(s)/X_q(s)$ and $G(s)$. To bring out the influence of these differences among the models on the damping performance of swing-mode and torsional modes in an FSC compensated system, the following cases are considered.

- Without AVR: Since E_{fd} is constant, the influence of $G(s)$ does not figure in the model performance. Thus, the OI- and OIR/EC(Canay)-models are identical and differ from EC-model only with respect to $X_d(s)/X_q(s)$.
- With AVR: This case considers a single time-constant static exciter (see Appendix A for the exciter parameters). Here, the influence of both $X_d(s)/X_q(s)$ and $G(s)$ are brought out.
- With PSS: Two types of PSS such as slip-signal and Delta-P-Omega PSS are considered (see Appendix A for the PSS parameters). This case accounts the effect of PSS-controllers in addition to the standard transfer functions.

TABLE II
FSC COMPENSATION FOR THE PERFECTLY TUNED CONDITIONS

Mode	Frequency (Hz)	x_{FC} (pu)
Torsional mode-4	32.368	0.18
Torsional mode-3	25.472	0.29
Torsional mode-2	20.221	0.38
Torsional mode-1	15.62	0.46

Eigenvalue analysis is carried out on MATLAB and time-domain simulations are performed on SIMULINK with step-size less than 10 μs employing trapezoidal method of integration. A perturbation in the form of a step change in the mechanical power of all the turbines is considered for applying the disturbance. In the time-domain simulations, the modal speed deviations [44]–[46] are evaluated to understand the behavior of a given mode. In an effort to calculate the modal speeds in the simulation responses, the modal speed deviation $\Delta\omega_{Ml}$ corresponding to mode l, is approximately obtained as follows:

$$\Delta\omega_{Ml} = v_l^T[\Delta\omega_{HP}, \Delta\omega_{IP}, \cdots \Delta\omega_{EXC}]^T$$

where v_l^T is a vector containing the left eigenvector components corresponding to individual angular speed deviations of the rotor masses of the turbine-generator system $(\Delta\omega_{HP}, \Delta\omega_{IP}, \cdots \Delta\omega_{EXC})$. It is to be noted that these eigenvectors are obtained corresponding to the unconnected mechanical system neglecting damping.

III. INFLUENCE OF GENERATOR MODELS ON TORSIONAL-DYNAMICS

In this section, influence of the synchronous machine models on the torsional dynamics has been investigated. It is known that IEEE FBS is characterized by five torsional modes of which the torsional mode-5 is uncontrollable by any means due to its high value of modal inertia [6]. Therefore analysis of the damping performance is restricted to torsional mode-1 to mode-4. Case studies are performed by varying FSC compensation around the *perfectly tuned* conditions for each of the torsional modes, assuming full-load conditions (i.e., $P_g = 1.0$ pu). For example, to study the damping performance of mode-2, FSC compensation is varied in a smaller step around $x_{FC} = 0.38$ pu (see Table II).

A. Damping Performance of Torsional Mode-1

In this section, damping performance of torsional mode-1 is studied for various degrees of FSC compensation. Note that mode-1 is perfectly tuned for $x_{FC} = 0.46$ pu (see Table II) and

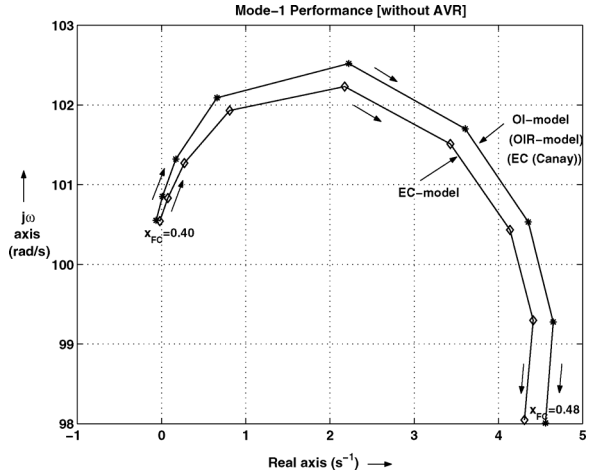

Fig. 2. Root-locus plot of mode-1 in the absence of AVR.

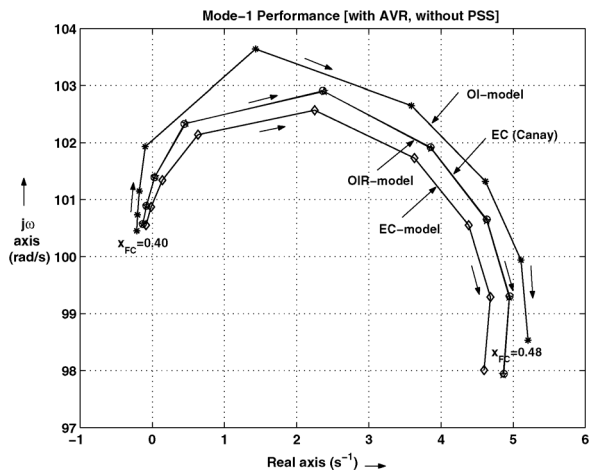

Fig. 3. Root-locus plot of mode-1 in the presence of AVR.

FSC compensation is varied from $x_{FC} = 0.40$ pu to $x_{FC} = 0.48$ pu in step of 0.01 pu.

1) Mode-1 Performance Without AVR: The root-locus plot of the mode-1 without AVR is as shown in Fig. 2. The figure shows that the OI-model and OIR/EC(Canay)-model behave identically since $G(s)$ is ineffective and $X_d(s)$ is the same in both the models. From the figure it is also evident that difference in $X_d(s)$ among the EC-model and the OI [or OIR/EC(Canay)]-model contributes to deviation in the damping.

2) Mode-1 Performance With AVR: Fig. 3 shows the root-locus plot of the mode-1 when AVR is enabled. From the figure it can be seen that the OIR/EC(Canay)-model diverges significantly from the OI-model, though these two models differ only in $G(s)$. The EC-model predictions deviate further due to the difference in both $X_d(s)$ and $G(s)$, from the other two models. Further, it can be seen that, since the OIR/EC(Canay)-model represents $G(s)$ slightly close to that of the EC-model, the characteristic tends to shift towards the EC-model though the magnitude of deviation is relatively large.

3) Mode-1 Performance With PSS: In this case, Delta-P-Omega PSS is enabled and the influence of the generator models on the damping performance of mode-1 is investigated. From Fig. 4 it is evident that the performance is quite similar to that in Fig. 3, demonstrating that the presence of PSS does not influence the behavior appreciably.

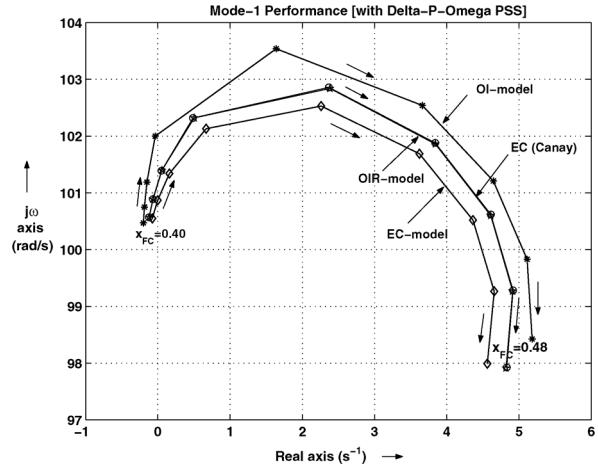

Fig. 4. Root-locus plot of mode-1 in the presence of Delta-P-Omega PSS.

TABLE III
MODE-1: $x_{FC} = 0.41$ pu, WITH DELTA-P-OMEGA PSS

OI-model	EC-model	OIR-model	EC(Canay)
-0.186± j100.75	-0.002± j100.87	-0.069± j100.89	-0.066± j100.89

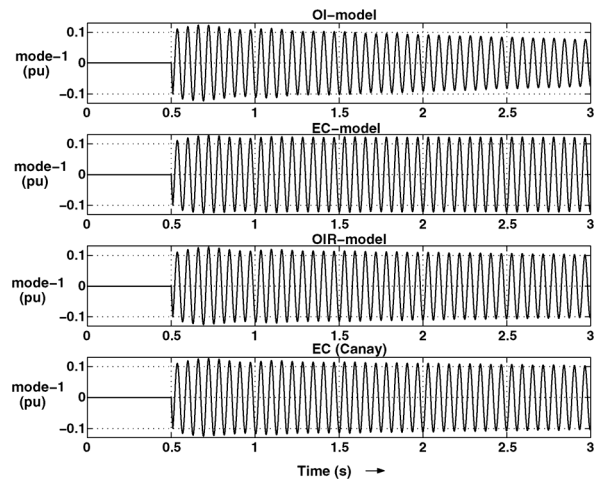

Fig. 5. Mode-1 performance, $x_{FC} = 0.41$ pu, with Delta-P-Omega PSS.

The above study has been repeated with a slip-signal PSS. The inferences are found to be similar to those with Delta-P-Omega PSS.

4) An Example—Mode-1 Damping With Delta-P-Omega PSS for $x_{FC} = 0.41$ pu: For this case, Table III lists the eigenvalue for mode-1 with various generator models. From the table it is clear that the difference in the damping caused by the models is significantly large at this compensation level. These inferences are further verified by the time-domain simulations with each of the models (see Fig. 5).

B. Damping Performance of Rest of the Torsional Modes

In this section, influence of the generator models on the damping performance of rest of the torsional modes is investigated. From the case studies it is found that differences in damping performances offered by the different generator

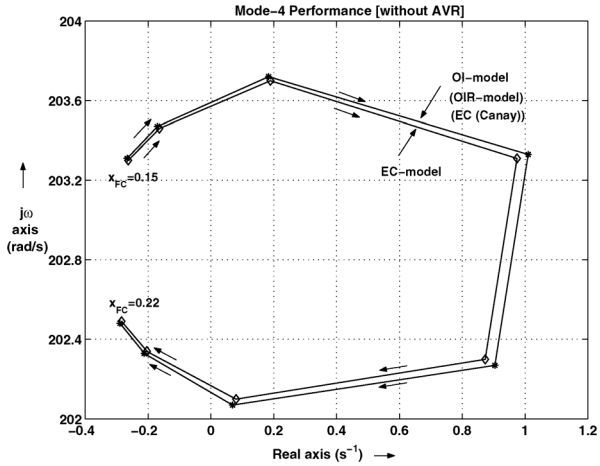

Fig. 6. Root-locus plot of mode-4 in the absence of AVR.

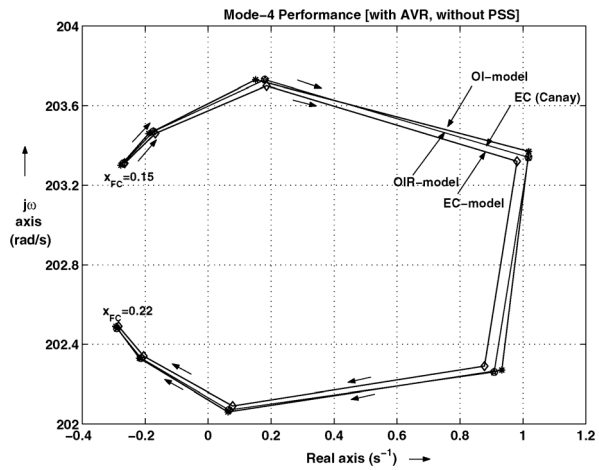

Fig. 7. Root-locus plot of mode-4 in the presence of AVR.

models for mode-2 and mode-3 are moderate. On the other hand, all of the generator models perform quite similarly with respect to mode-4 in all cases. This is evident from Fig. 6, wherein the divergence of the EC-model from the OI [or OIR/EC(Canay)]-model is negligible in a case where AVR is disabled [though the models differ in $X_d(s)$]. Further, it is also found that the difference in $G(s)$ does not contribute appreciably in the damping of mode-4. This is evident in Fig. 7. Similar observations are made even when PSS is enabled.

From the study of the damping performance of torsional modes with different generator models, the following observations are made:

- The synchronous machine models perform significantly differently when the FSC compensation level is quite high which corresponds to mode-1.
- The influence of $G(s)$ is significant in comparison to $X_d(s)$. This is prominently seen with respect to mode-1.

IV. Influence of Generator Models on Slip-Signal PSS-Torsional Interactions

In this section, the influence of the generator models on the well known slip-signal PSS-torsional interaction (TI) is analyzed. A slip-signal PSS *without torsional filter* is considered.

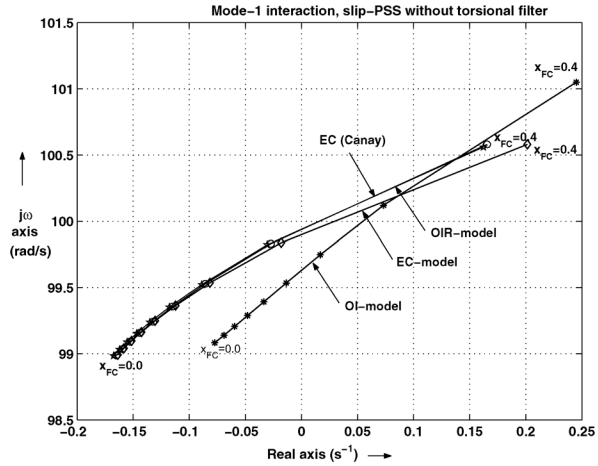

Fig. 8. Root locus of mode-1 to demonstrate slip-signal-torsional-interaction.

The loading level of $P_g = 1.0$ pu is assumed. The FSC compensation is varied from $x_{FC} = 0$ pu (i.e., no compensation) to $x_{FC} = 0.4$ pu (i.e., 80% compensation) in steps of 0.05 pu. From the study following observations are made (see Fig. 8).

- With any generator model, the mode-1 damping reduces with an increase in FSC compensation.
- With the OI-model, the mode-1 becomes unstable when the series compensation is 56% (i.e., $x_{FC} = 0.28$ pu) and above. Whereas with the EC-model and the OIR/EC(Canay)-model, the mode-1 instability is seen only when the series compensation is above 72% and 74%, respectively.
- Since the OI-model and the OIR/EC(Canay)-model differ only in terms of $G(s)$, and in this case, the EC-model behaves similar to the OIR/EC(Canay)-model, we can conclude that the influence of the standard transfer function $G(s)$ dominates here also, especially with respect to mode-1.

A. Example—Slip-Signal TI for an FSC Compensation, $x_{FC} = 0.35$ pu

Table IV lists the eigenvalues for an FSC compensation of $x_{FC} = 0.35$ pu. From the table it can be seen that mode-1 is unstable with the OI-model. However, with the EC-model and OIR/EC(Canay)-model, mode-1 remains stable as slip-signal torsional interaction starts only when the level of FSC compensation is above $x_{FC} = 0.35$ pu. These observations are verified by the time-domain simulation as well-see Fig. 9. Note that the simulation plot for the OIR/EC(Canay)-model is not shown separately since it almost matches with that for the EC-model.

V. Influence of Generator Models on Damping Performance of Swing-Mode

In this section, case studies are carried out to investigate the influence of the generator models on the damping performance of the swing-mode for various degrees of series compensation of the transmission line. FSC compensation has been varied from $x_{FC} = 0$ pu (i.e., no compensation) to $x_{FC} = 0.45$ pu (i.e.,

TABLE IV
EIGENVALUES: SLIP-SIGNAL TORSIONAL INTERACTION AT $x_{FC} = 0.35$ pu

OI-model	EC-model	OIR-model	EC(Canay)
-4.704± j616.65	-4.631± j616.63	-4.709± j616.62	-4.709± j616.62
-2.365± j137.03	-3.135± j136.76	-2.757± j136.73	-2.767± j136.72
-0.347± j202.80	-0.361± j202.81	-0.362± j202.81	-0.362± j202.81
-0.632± j160.25	-0.633± j160.30	-0.638± j160.30	-0.638± j160.30
0.019± j127.29	0.012± j127.23	0.005± j127.23	0.004± j127.23
0.073± j100.13	-0.018± j99.84	-0.027± j99.83	-0.030± j99.82
-2.155± j11.64	-1.991± j12.29	-2.540± j11.85	-2.557± j11.85

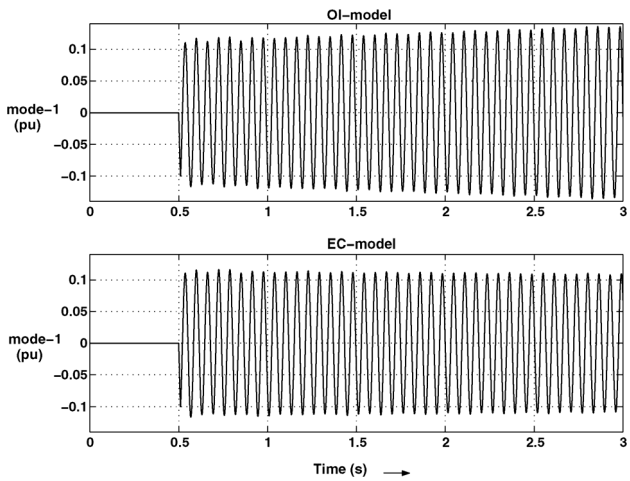

Fig. 9. Slip-signal torsional interaction, $x_{FC} = 0.35$ pu.

90% compensation) in steps of 0.05 pu. All the studies are conducted at fully-loaded condition (i.e., $P_g = 1.0$ pu).

A. Swing-Mode Damping Performance Without AVR

The root-locus plot of the swing-mode is shown in Fig. 10 when AVR is disabled. The figure shows that the OI-model and the OIR/EC(Canay)-model behave identically for the reason which is explained previously. From the figure it is also seen that eigen-predictions of the EC-model diverge significantly from the OI [or OIR/EC(Canay)]-model due to the influence of $X_d(s)$ alone.

B. Swing-Mode Damping Performance With AVR

Fig. 11 shows the swing-mode performance of the system with each of the generator models when AVR is enabled. From the figure it can be seen that all the models differ significantly. Further, it can be noted that when $G(s)$ is made effective by considering AVR, the OIR/EC(Canay)-model tends to shift towards the EC-model by reducing the difference by nearly 50% with respect to that indicated in Fig. 10. This clearly shows the dominance of $G(s)$ in the swing-mode performance of synchronous machine models.

C. Swing-Mode Damping Performance With PSS

Swing-mode performance of an FSC compensated system in the presence of PSS, with the OI-model, is reported in [47]. It is shown that the type of PSS has a major impact on the damping

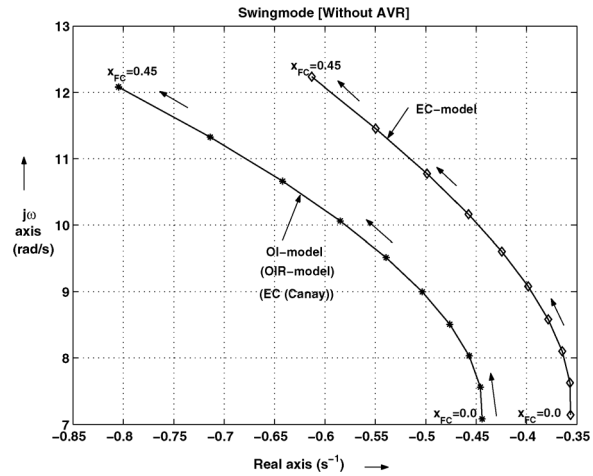

Fig. 10. Root-locus plot of swing-mode in the absence of AVR.

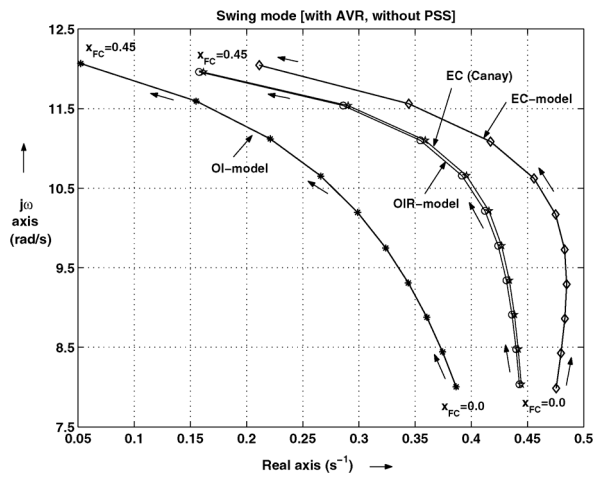

Fig. 11. Root-locus plot of swing-mode in the presence of AVR.

of swing-mode. In this section, an investigation is done to understand the effect of different synchronous machine models on the swing-mode damping.

To start with, a slip-signal PSS is considered. In this case, the following observations are made (see Fig. 12):

- For each of the generator models, the damping for the swing-mode improves with the series compensation up to a certain level of compensation, (i.e., $x_{FC} = 0.2$ pu for the OI-model, $x_{FC} = 0.1$ pu for the EC-model and $x_{FC} = 0.15$ pu for the OIR/EC(Canay)-model), beyond which an increase in the compensation worsens the damping unlike in a case where the PSS is absent.
- With the OI-model, an increase in the series compensation beyond 84% results in an unstable swing-mode. With the EC-model and the OIR/EC(Canay)-model, the swing-mode destabilizes when the series compensation is just above 56% and 64%, respectively.
- At low levels of compensation, the OIR/EC(Canay)-model behaves similar to that of the OI-model. This shows that the influence of $G(s)$ is small. This also implies that the difference in $X_d(s)$ is the major cause for the behavior of the EC-model. However, as the compensation level increases, the $G(s)$ influence dominates as in the torsional mode case.

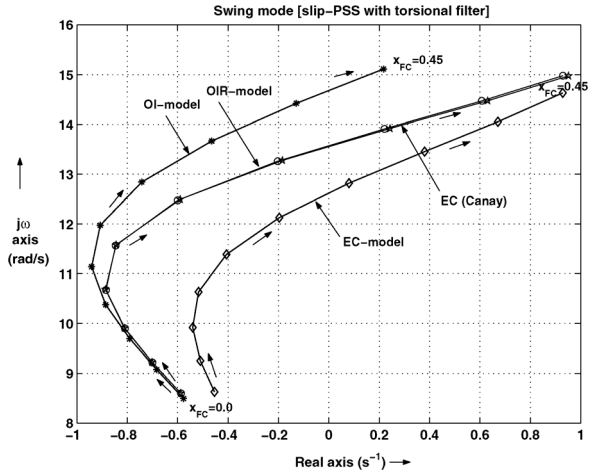

Fig. 12. Root-locus of swing-mode in the presence of slip-signal PSS.

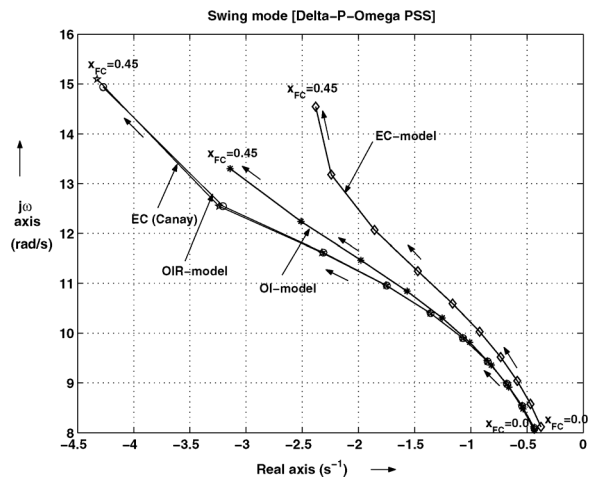

Fig. 13. Root-locus of swing-mode in the presence of Delta-P-Omega PSS.

The above study has been repeated with a Delta-P-Omega PSS. From Fig. 13 it can be seen that with any generator model, as the FSC compensation increases, the damping of the swing-mode continues to increase unlike that with a slip-signal PSS. It is seen that though $G(s)$ influence dominates as the compensation level increases, the direction of its effect reverses with respect to that in slip-signal PSS case. Further, it should be noted that the difference in the swing-mode damping predictions among the models is relatively small when compared to that with a slip-signal PSS.

D. Example—Swing-mode Damping With PSS for $x_{FC} = 0.35$ pu

For this case, the swing-mode has been listed in Table V for each of the PSS. From the table it can be seen that with slip-signal PSS, the stable swing-mode offered by the OI-model becomes unstable with the EC-model and the OIR/EC(Canay)-model.

These observations are further verified by time-domain simulations-see Fig. 14. From the table it is also seen that unlike with slip-signal PSS, all the models offer a positive damping in the same range with Delta-P-Omega PSS.

TABLE V
SWING-MODE: $x_{FC} = 0.35$ pu AND $P_g = 1.0$ pu

PSS	OI-model	EC-model	OIR-model	EC (Canay)
Slip	-0.46± j13.66	0.38± j13.45	0.22± j13.91	0.24± j13.92
DPO	-1.98± j11.46	-1.86± j12.06	-2.31± j11.62	-2.32± j11.62

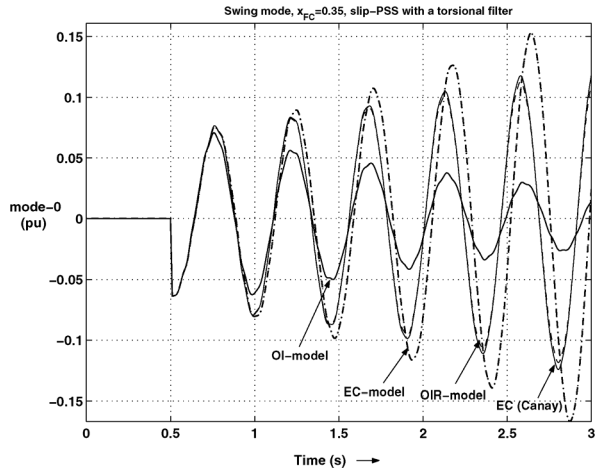

Fig. 14. Swing-mode for slip-signal PSS, $x_{FC} = 0.35$ pu.

TABLE VI
SWING-MODE: FSC COMPENSATION OF $x_{FC} = 0.35$ pu AND $P_g = 0.5$ pu

PSS	OI-model	EC-model	OIR-model	EC (Canay)
Slip	-2.35± j12.60	-1.58± j13.10	-2.55± j13.34	-2.56± j13.37
DPO	-2.46± j10.72	-2.38± j11.04	-2.65± j10.64	-2.65± j10.64

E. Effect of Loading Level on Swing-Mode Damping With PSS for $x_{FC} = 0.35$ pu

In this section, effect of loading level on the swing-mode performance in the presence of PSS is analysed. Table VI lists the swing-mode for $x_{FC} = 0.35$ pu with $P_g = 0.5$ pu for all the models. By comparing the results with that in Table V, it can be said that at reduced power levels the difference in the swing-mode damping offered by the models is relatively lower than that at full-load conditions.

F. GEP Transfer Function-Based Analysis

The above inferences about the change in the swing-mode damping with generator models in the presence of PSS, can be better explained with the help of a GEP transfer function, i.e., $GEP(s) = \Delta T_e(s)/\Delta V_s(s)$-based analysis [7], [48]. The phase angle response of the augmented $GEP(s)$ which is the combined phase response of the $GEP(s)$ and the PSS-transfer function, provides better insight into the behavior.

Fig. 15 shows the phase angle response of the augmented $GEP(s)$ (denoted as the phase angle lag ϕ_a) with slip-signal PSS for an FSC compensation, $x_{FC} = 0.35$ pu. From the figure, it can be said that

- With the OI-model, ϕ_a is well within 60° at swing-mode frequency.
- The ϕ_a is found to be slightly more than 90° for the EC-model and the OIR/EC(Canay)-model, resulting in a negative damping of the swing-mode.

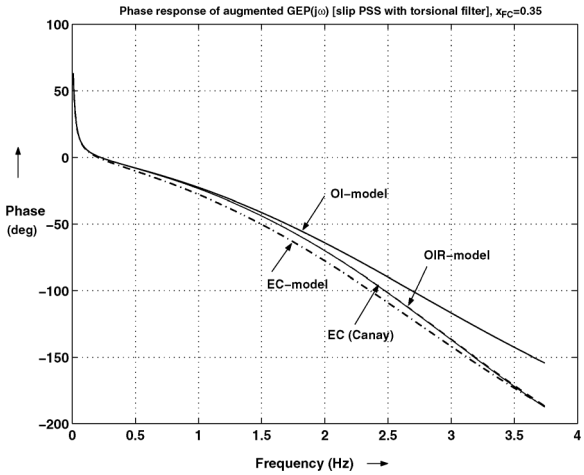

Fig. 15. Phase response of the augmented $GEP(s)$ [slip-signal PSS], $x_{FC} = 0.35$ pu.

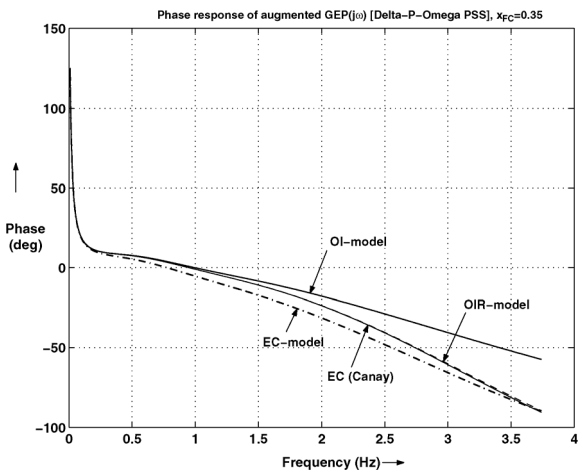

Fig. 16. Phase response of the augmented $GEP(s)$ [Delta-P-Omega PSS], $x_{FC} = 0.35$ pu.

However, with Delta-P-Omega PSS, ϕ_a is much less than 90° for all the generator models-see Fig. 16. Therefore, the swing-mode does not become unstable with any of the models.

VI. Conclusions

In this paper, the SSR performance of the IEEE FBS is studied employing four types of models for the generator: EC-model, EC(Canay)-model, OI-model and OIR-model. The case studies presented related to the swing-mode demonstrate that a slip-signal PSS designed to provide good damping with the OI-model worsens the swing-mode stability when the generator model is changed to the EC-model or the OIR/EC(Canay)-model; however, when a Delta-P-Omega PSS is used all models behave similarly. This is found to be due to the following reasons:

1) At low series compensation levels, the influence of $X_d(s)$ dominates, whereas at high series compensation levels, the difference in $G(s)$ is prominent.
2) This in turn alters the PSS-compensator angle requirements as evident from the augmented $GEP(s)$ plots.

TABLE VII
Generator Standard Parameters

x_d= 1.79	x'_d= 0.169	x''_d=0.135	T'_{do}=4.3 s	$T''_{d\rho}$=0.032 s
x_q= 1.71	x_q= 0.228	x''_q=0.2	T'_{qo}=0.85 s	T'_{qo}=0.05 s
x_l= 0.13	R_a=0			

This implies that when slip-signal PSS is used, it is required to re-tune the PSS depending upon the compensation level and the generator model employed. However, if Delta-P-Omega PSS is used, such a constraint does not exist.

The case studies presented related to the torsional modes demonstrate that the models perform differently even with respect to torsional modes and these differences are significant as we move towards lower torsional modes. It should be noted that the differences between the EC-models and the OI-models disappear if one uses the EC(Canay)-model and the OI(refined)-model for the generator. It is felt that such a study definitely helps the researchers and academicians to know the model behavior when it is required to design/tune damping controllers and to compare results obtained on different computational platforms.

Appendix A
System Data

A. IEEE FBS Data

Generator standard parameters are listed in Table VII as specified in [42]. The mechanical damping (both self and mutual) data are also listed as given in [6]. All resistances and reactances are in per unit.

Self damping	$D_{HP} = D_{IP} = D_{LA} = D_{LB} = 0.2$, $D_G = 0$
Mutual damping	$D_{HI} = D_{IA} = D_{AB} = D_{BG} = 0.3$, $D_{GE} = 0.005$.
Network data	$R = 0.02$, $x_T = 0.14$, $x_L = 0.5$, $x_{SYS} = 0.06$.

B. Exciter and PSS Data

Exciter: Single-time-constant static exciter is with $K_A = 200$ and $T_A = 0.025$ s.

Slip-Signal PSS: The slip-signal PSS uses a phase-lead circuit (with center frequency, $f_m = 2.37$ Hz and angle lead, $\phi_m = 22.29°$) and a torsional filter (with $\zeta = 0.6$ and $\omega_n = 22$ rad/s). The gain set to $K_s = 4.5$ so that the swing-mode damping factor is about 5% for an FSC compensation of $x_{FC} = 0.3$ pu.

Delta-P-Omega PSS: The parameters are similar to that of slip-signal PSS with gain $K_s = 1.25$ so that the swing-mode damping is the same as mentioned above.

Appendix B
Classical Data Conversion Procedure

The EC-model involves the determination of the basic parameters such as field/damper winding resistances and their respective leakage reactances. Employing the classical data conversion procedure [5], we have

$$
\begin{aligned}
x_{ad} &= x_d - x_l \\
\frac{1}{x_{lfd}} &= \frac{1}{x'_d - x_l} - \frac{1}{x_{ad}} \\
\frac{1}{x_{lhd}} &= \frac{1}{x''_d - x_l} - \frac{1}{x'_d - x_l} \\
R_{fd} &= \frac{x_{ad} + x_{lfd}}{\omega_B T'_{do}} \\
R_{hd} &= \frac{x_{ad}x_{lfd} + x_{lfd}x_{lhd} + x_{lhd}x_{ad}}{\omega_B T''_{do}(x_{ad} + x_{lfd})}.
\end{aligned}
$$

Using the standard parameters given in Table VII, the basic parameters obtained for the d-axis are listed below (in pu):

$$
x_{ad} = 1.66, \quad x_{lfd} = 0.039938, \quad x_{lhd} = 0.0057353
$$
$$
R_{fd} = 0.0010487, \quad R_{hd} = 0.0037083.
$$

Appendix C
Determination of Short-Circuit Time-Constants

By relating (2) and (5) we can obtain the following relationships [32]:

$$
T'_d \frac{x_d}{x'_d} + T''_d \left(1 - \frac{x_d}{x'_d} + \frac{x_d}{x''_d}\right) = T'_{do} + T''_{do} \tag{6}
$$
$$
T'_d T''_d \left(\frac{x_d}{x''_d}\right) = T'_{do} T''_{do}. \tag{7}
$$

The above equations permit us to calculate short-circuit time-constants from the open-circuit time constants. Thus we get $T'_d = 0.4$ s, $T''_d = 0.0259$ s.

Appendix D
Determination of T_{kd} for OIR-Model

An approximate value of T_{kd} can be obtained as [32]

$$
T_{kd} = \frac{b}{c} \tag{8}
$$

with

$$
b = a\frac{x_{ad}\,(x''_d - x_l)}{ax_d + x_l x_{ad} - (a + x_{ad})x''_d}
$$
$$
c = \frac{1}{T''_d}\left(b + \frac{ax_l x_{ad}}{x_l x_{ad} + ax_d}\right) \text{ and } a = x_{ad}\frac{x'_d - x_l}{x_d - x'_d}.
$$

Using the above equations, we obtain $T_{kd} = 0.00416$ s.

Appendix E
EC (Canay) Parameters

Following the Canay data conversion procedure and with $x_c = x_l$ as in [39], the basic parameters for the EC (Canay)-model for the d-axis are obtained as listed below (in pu):

$$
x_{dc} = x_{ad} = 1.66, \quad x_{lfd} = 0.061789, \quad x_{lhd} = 0.0054581
$$
$$
R_{fd} = 0.0014068, \quad R_{hd} = 0.0040699.
$$

Acknowledgment

The authors would like to thank Prof. A.M. Kulkarni, Department of Electrical Engineering, IIT Bombay, India for his valuable suggestions.

References

[1] E. W. Kimbark, "Improvement of system stability by switched series capacitors," *IEEE Trans. Power App. Syst.*, vol. PAS-85, no. 2, pp. 180–188, Feb. 1966.

[2] IEEE SSR Working Group, "Countermeasures to subsynchronous resonance problems," *IEEE Trans. Power App. Syst.*, vol. PAS-99, no. 5, pp. 1810–1818, Sep. 1980.

[3] P. M. Anderson, B. L. Agrawal, and J. E. Van Ness, *Subsynchronous Resonance in Power Systems*. Piscataway, NJ, USA: IEEE Press, 1990.

[4] IEEE Committee Report, "Reader's guide to subsynchronous resonance," *IEEE Trans. Power Syst.*, vol. 7, no. 1, pp. 150–157, Feb. 1992.

[5] P. Kundur, *Power System Stability and Control*. New York, NY, USA: McGraw-Hill, 1994.

[6] K. R. Padiyar, *Analysis Of Subsynchronous Resonance In Power Systems*. Norwell, MA, USA: Kluwer, 1999.

[7] K. R. Padiyar, *Power System Dynamics—Stability and Control*. Hyderabad, India: BS Publications, 2002.

[8] A. I. Megahed and O. P. Malik, "Synchronous generator internal fault computation and experimental verification," *Proc. Inst. Elect. Eng., Gen. Transm., Distrib.*, vol. 145, pp. 604–610, Sep. 1998.

[9] K. H. Chan, E. Acha, M. Madrigal, and J. A. Parle, "The use of direct time-phase domain synchronous generator model in standard EMTP-type industrial packages," *IEEE Power Eng. Rev.*, vol. 21, no. 6, pp. 63–65, Jun. 2001.

[10] K. H. Chan, J. A. Parle, and E. Acha, "Real-time transient simulation of multimachine power system networks in the phase domain," *Proc. Inst. Elect. Eng., Gen., Transm., Distrib.*, vol. 151, no. 2, pp. 192–200, Mar. 2004.

[11] L. Quéval, M. Sekino, and H. Ohsaki, "A coupled FE phase-domain model for superconducting synchronous machine," *IEEE Trans. Appl. Supercond.*, vol. 22, no. 3, p. 5200804, Jun. 2012.

[12] L. Wang and J. Jatskevich, "A phase-domain synchronous machine model with constant equivalent conductance matrix for EMTP-type solution," *IEEE Trans. Energy Convers.*, vol. 28, no. 1, pp. 191–202, Mar. 2013.

[13] S. D. Pekarek, O. Wasynczuk, and H. J. Hegner, "An efficient and accurate model for the simulation and analysis of synchronous machine/converter systems," *IEEE Trans. Energy Convers.*, vol. 13, no. 1, pp. 42–48, Mar. 1998.

[14] L. Wang and J. Jatskevich, "A voltage-behind-reactance synchronous machine model for the EMTP-type solution," *IEEE Trans. Power Syst.*, vol. 21, no. 4, pp. 1539–1549, Nov. 2006.

[15] L. Wang and J. Jatskevich, "Magnetically-saturable voltage-behind-reactance synchronous machine model for the EMTP-type solution," *IEEE Trans. Power Syst.*, vol. 26, no. 4, pp. 2355–2363, Nov. 2011.

[16] M. Chapariha, L. Wang, J. Jatskevich, H. W. Dommel, and S. D. Pekarek, "Constant-parameter RL-branch equivalent circuit for interfacing AC machine models in state-variable-based simulation packages," *IEEE Trans. Energy Convers.*, vol. 27, no. 3, pp. 634–645, Sep. 2012.

[17] U. Karaagac, J. Mahseredjian, I. Kocar, and O. Saad, "An efficient voltage-behind-reactance formulation-based synchronous machine model for electromagnetic transients," *IEEE Trans. Power Del.*, vol. 28, no. 3, pp. 1788–1795, Jul. 2013.

[18] U. Karaagac, J. Mahseredjian, O. Saad, and S. Dennetiére, "Synchronous machine modeling precision and efficiency in electromagnetic transients," *IEEE Trans. Power Del.*, vol. 26, no. 2, pp. 1072–1082, Apr. 2011.

[19] U. Karaagac, J. Mahseredjian, and O. Saad, "An efficient synchronous machine model for electromagnetic transients," *IEEE Trans. Power Del.*, vol. 26, no. 4, pp. 2456–2465, Oct. 2011.

[20] Y. Cui, H. W. Dommel, and W. Xu, "A comparative study of two synchronous machine modeling techniques for EMTP simulation," *IEEE Trans. Energy Convers.*, vol. 19, no. 2, pp. 462–463, Jun. 2004.

[21] L. Wang, J. Jatskevich, and H. W. Dommel, "Re-examination of synchronous machine modeling techniques for electromagnetic transient simulations," *IEEE Trans. Power Syst.*, vol. 22, no. 3, pp. 1221–1230, Aug. 2007.
[22] F. Therrien, L. Wang, J. Jatskevich, and O. Wasynczuk, "Efficient explicit representation of AC machines main flux saturation in state-variable-based transient simulation packages," *IEEE Trans. Energy Convers.*, vol. 28, no. 2, pp. 380–393, Jun. 2013.
[23] Alternative Transients Programs, 2007, ATP-EMTP, ATP User Group. West Linn, OR, USA [Online]. Available: http://www.emtp.org
[24] MicroTran Reference Manual, 1997, MicroTran Power System Analysis Corp. Vancouver, BC, Canada [Online]. Available: http://www.microtran.com
[25] PSCAD/EMTDC (2007), Manitoba HVDC Research Centre and RTDS Technologies Inc. Winnipeg, MB, Canada [Online]. Available: http://www.pscad.com
[26] Electromagnetic Transient Program, 2007, EMTP RV, CEA Technologies Inc. Columbia, MD, USA [Online]. Available: http://www.emtp.com
[27] Simulink Dynamic System Simulation Software Users Manual, MathWorks, Inc. Natick, MA, USA, 2009 [Online]. Available: http://www.mathworks.com
[28] EUROSTAG: Software for Simulation of Large Electric Power Systems, Tractebel Energy Engineering. Brussels, Belgium, Release 4.5, 2012 [Online]. Available: http://www.eurostag.be
[29] J. G. Slootweg, J. Persson, A. M. van Voorden, G. C. Paap, and W. L. Kling, "A study of the eigenvalue analysis capabilities of power system dynamics simulation software," in *Proc. 14th Power Syst. Computation Conf.*, Sevilla, Spain, Jun. 2002.
[30] DIgSILENT PowerFactory Manual Version 14.0, DIgSILENT GmbH. Gomaringen, Germany, 2010.
[31] PowerWorld, 2010 [Online]. Available: http://www.powerworld.com/transientquickstart.asp
[32] *IEEE Guide for Synchronous Generator Modeling Practices and Applications in Power System Stability Analysis*, IEEE Std. 1110-2002, Nov. 2003.
[33] N. Watson and J. Arrillaga, *Power Systems Electromagnetic Transients Simulation*. London, U.K.: Inst. Elect. Eng., 2003.
[34] IEEE Task Force on Interfacing Techniques for Simulation Tools, "Methods of interfacing rotating machine models in transient simulation programs," *IEEE Trans. Power Del.*, vol. 25, no. 2, pp. 891–903, Apr. 2010.
[35] *IEEE Guide for Test Procedures for Synchronous Machines*, IEEE Std. 115-2009, May 2010.
[36] P. M. Anderson and A. A. Fouad, *Power System Control and Stability*. Ames, IA, USA: Iowa State Univ. Press, 1977.
[37] P. W. Sauer and M. A. Pai, *Power System Dynamics and Stability*. Upper Saddle River, NJ, USA: Prentice Hall, 1998.
[38] H. W. Dommel, *EMTP Theory Book*. Vancouver, BC, Canada: MicroTran Power System Analysis Corporation, May 1992.
[39] I. M. Canay, "Determination of model parameters of synchronous machines," *Proc. Inst. Elect. Eng.*, vol. 130, no. 2, pp. 86–94, Mar. 1983.
[40] H. W. Dommel and I. I. Dommel, "Discussion to"Synchronous machine parameters from sudden-short tests by back-solving"," *IEEE Trans. Energy Convers.*, vol. 4, no. 2, pp. 232–233, Jun. 1989.
[41] A. M. Kulkarni, Power System Dynamics and Control [Online]. Available: http://nptel.iitm.ac.in/courses/108101004/
[42] IEEE SSR Task Force, "First benchmark model for computer simulation of subsynchronous resonance," *IEEE Trans. Power App. Syst.*, vol. PAS-96, no. 5, pp. 1565–1572, Sep./Oct. 1977.
[43] F. Zhang and Z. Xu, "Effect of exciter and PSS on SSR damping," in *Proc. IEEE PES General Meeting*, Jun. 2007, pp. 1–7.
[44] G. D. Jennings, R. G. Harley, and D. C. Levy, "Sensitivity of subsynchronous resonance predictions to turbo-generator modal parameter values and to omitting certain active subsynchronous modes," *IEEE Trans. Energy Convers.*, vol. 2, no. 3, pp. 470–479, Sep. 1987.
[45] S. R. Joshi and A. M. Kulkarni, "Analysis of SSR performance of TCSC control schemes using a modular high bandwidth discrete-time dynamic model," *IEEE Trans. Power Syst.*, vol. 24, no. 2, pp. 840–848, May 2009.
[46] D. Rai, S. O. Faried, G. Ramakrishna, and A. A. Edris, "An SSSC-based hybrid series compensation scheme capable of damping subsynchronous resonance," *IEEE Trans. Power Del.*, vol. 27, no. 2, pp. 531–540, Apr. 2012.
[47] M. K. Shashidhara and K. N. Shubhanga, "Some aspects of power system stabilizer performance in subsynchronous resonance study," in *Proc. Int. Conf. Power and Energy Systems (ICPS)*, IIT Chennai, India, Dec. 2011, pp. 1–6.
[48] E. V. Larsen and D. A. Swann, "Applying power system stabilizers, Part I; General concepts, Part II; Performance objectives and tuning Concepts, Part III; Practical considerations," *IEEE Trans. Power App. Syst.*, vol. PAS-100, no. 6, pp. 3017–3046, Jun. 1981.

Shashidhara M. Kotian received the B.E. degree in electrical engineering and the M.Tech. degree in power systems from the National Institute of Technology Karnataka, Surathkal, India, in 2006 and 2010, respectively, and is currently pursuing the Ph.D. degree at the NITK, Surathkal, India.

K. N. Shubhanga received the B.E. degree in electrical engineering and the M.Tech. degree in power systems from Mangalore University, India, in 1991 and 1994, respectively, and Ph.D. degree from the Indian Institute of Technology, Bombay, in 2003.

He is currently an Associate Professor at the National Institute of Technology Karnataka, Surathkal, India. His research interests are in the areas of FACTS and power system dynamics.